NANO EXPRESS

Open Access

CrossMark

Numerical Study on Convective Heat Transfer Enhancement in Horizontal Rectangle Enclosures Filled with Ag-Ga Nanofluid

Cong Qi[*], Liyuan Yang and Guiqing Wang

Abstract

The natural convection heat transfer of horizontal rectangle enclosures with different aspect ratios ($A = 2$:1 and $A = 4$:1) filled with Ag-Ga nanofluid (different nanoparticle volume fractions $\varphi = 0.01$, $\varphi = 0.03$, $\varphi = 0.05$ and radiuses $r = 20$ nm, $r = 40$ nm, $r = 80$ nm) at different Rayleigh numbers ($Ra = 1 \times 10^3$ and $Ra = 1 \times 10^5$) is investigated by a two-phase lattice Boltzmann model. It is found that the Nusselt number enhancement ratios of two enclosures ($A = 2$:1 and $A = 4$:1) filled with Ag-Ga nanofluid ($r = 20$ nm) are the same compared with those of the water at the corresponding aspect ratio enclosure. The more flat horizontal rectangular enclosure ($A = 4$:1) has the higher Nusselt number than the less flat horizontal rectangular enclosure ($A = 2$:1). It is also found that Nusselt number increases with the decreasing nanoparticle radius. Nusselt number enhancement ratios for every nanoparticle radius reducing by half at high Rayleigh number are higher than those at low Rayleigh number in most cases. The interaction forces between particles are also investigated in this paper. It is found that the Brownian force F_B is about two magnitudes greater than that of drag force F_D, and the value of driving force F_S in $A = 4$:1 enclosure is about twice the value of driving force F_S in $A = 2$:1 enclosure while other forces are almost the same.

Keywords: Nanofluid, Natural convection, Heat transfer enhancement, Two-phase lattice Boltzmann method

Background

Heat transfer enhancement attracts more and more people's attention. One method is to improve the structure of the heat exchanger, and another method is to find new fluid with higher heat transfer performance instead of the common fluid. People have studied the structures of the heat exchangers for many years. About the heat transfer medium, since the nanofluid with high thermal conductivity is prepared, the thermal properties [1–3] and heat transfer performance [4–9] of nanofluid are studied by more and more researchers.

Natural convection heat transfer is an important heat transfer process. The natural convection heat transfer characteristics of nanofluid have been widely investigated by experimental and numerical methods respectively.

Natural convection heat transfer characteristics of nanofluid are experimentally investigated by many researchers. Ho et al. [10] experimentally investigated the natural convection heat transfer of Al_2O_3-water nanofluid in different size enclosures respectively, and the effects of nanoparticle volume fraction and Rayleigh number on the natural convection heat transfer of nanofluid are discussed. Heris et al. [11–13] experimentally investigated the laminar flow convective heat transfer of CuO-water, Al_2O_3-water, and Cu-water nanofluid in a circular tube respectively. Hu et al. [14] experimentally investigated the natural convection heat transfer of TiO_2-water nanofluid with different nanoparticle mass fractions, and the effects of Rayleigh number on natural convection heat transfer are discussed. Sommers et al. [15] experimentally investigated the convection heat transfer of Al_2O_3-propanol nanofluid through a copper pipe, and the effects of heat rate on the convection heat transfer are discussed.

* Correspondence: qicong@cumt.edu.cn
School of Electrical and Power Engineering, China University of Mining and Technology, Xuzhou 221116, China

Qi *et al. Nanoscale Research Letters* (2017) 12:326

Page 2 of 10

In addition to the experimental method, numerical simulation is also an important method to study the natural convection heat transfer of nanofluid. Many researchers have investigated the natural convection heat transfer of nanofluid by various numerical methods. He et al. [16] investigated the convection heat transfer of TiO$_2$-water nanofluid flowing through a straight tube by a single-phase method and a combined Euler and Lagrange method respectively. The effects of nanoparticle fraction, Reynolds number, and nanoparticle aggregated size on the convection heat transfer are discussed. Bianco et al. [17–19] investigated the convection flow of a circular tube filled with Al$_2$O$_3$-water nanofluid under different conditions respectively. Akbarinia et al. [20–22] investigated the mixed convection of Al$_2$O$_3$-water nanofluid in a horizontal curved tube, annulus and elliptic ducts respectively. Sheikholeslami et al. [23–27] investigated the natural convection heat transfer of various kinds of nanofluid under magnetic field and revealed the heat transfer enhancement mechanism of nanofluid. Qi et al. [28–30] investigated the natural convection heat transfer of Cu/Al$_2$O$_3$-water, Al$_2$O$_3$-water, and Cu-gallium in an enclosure by a lattice Boltzmann method respectively.

The above literatures made a great contribution to the researches on the effects of macro-factors (nanoparticle volume fraction, kinds of nanofluid, and so on) on the heat transfer of nanofluid. The effects of micro-factors (nanoparticle radius) on the heat transfer of nanofluid are needed to be studied. Hence, in our previous published paper [31], the natural convection heat transfer of a vertical rectangle enclosure (the left and the right walls are hot and cold walls, respectively, and other walls are adiabatic) filled with Cu-Ga nanofluid with various radius nanoparticles is investigated. In order to reveal the effects of different laying forms of the rectangle enclosure and different boundary conditions in the natural convection heat transfer of nanofluid with different nanoparticle radiuses, the natural convection of a horizontal rectangle enclosure (the left and
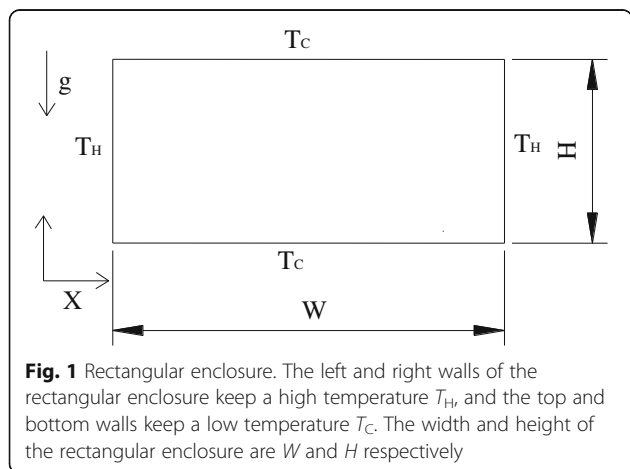

Fig. 1 Rectangular enclosure. The left and right walls of the rectangular enclosure keep a high temperature T_H, and the top and bottom walls keep a low temperature T_C. The width and height of the rectangular enclosure are W and H respectively

Table 1 Thermo-physical parameters. Thermo-physical parameters of liquid metal gallium and silver nanoparticle

Physical properties	Base fluid (Ga) [30]	Nanoparticle (Ag) [32]
ρ(kg/m^3)	6090	10,500
c_p(J/kg k)	429.9–0.275543 T	235
μ(m^2/s)	0.0018879	/
k(W m^{-1} K^{-1})	31	429

right walls are all hot walls, and other walls are all cold walls) filled with Ag-Ga nanofluid with various radius nanoparticles is investigated in this paper.

Methods

The natural convection of the horizontal rectangle enclosure filled with Ag-Ga nanofluid with various radiuses of nanoparticles is simulated by a two-phase lattice Boltzmann model. The two-phase lattice Boltzmann model for nanofluid has been developed by us in the previous published paper [31]. The main basic equations of the two-phase lattice Boltzmann model are given as follows:

The evolution equations and equilibrium distribution functions for velocity and temperature fields are given respectively as follows:

$$
\begin{aligned}
f_\alpha^\sigma(\boldsymbol{r} + \boldsymbol{e}_\alpha\delta_t, t + \delta_t) - f_\alpha^\sigma(\boldsymbol{r}, t) = &-\frac{1}{\tau_f^\sigma}\left[f_\alpha^\sigma(\boldsymbol{r}, t) - f_{\alpha^{\sigma eq}}(\boldsymbol{r}, t)\right] \\
&+ \frac{2\tau_f^\sigma - 1}{2\tau_f^\sigma} \cdot \frac{F_\alpha^\sigma \delta_t \boldsymbol{e}_\alpha}{B_\alpha c^2} + \delta_t F_{\alpha^{\sigma'}}
\end{aligned}
\tag{1}
$$

$$
f_\alpha^{\sigma eq} = \rho^\sigma w_\alpha \left[1 + \frac{\boldsymbol{e}_\alpha \cdot \boldsymbol{u}^\sigma}{c_s^2} + \frac{(\boldsymbol{e}_\alpha \cdot \boldsymbol{u}^\sigma)^2}{2c_s^4} - \frac{u^{\sigma 2}}{2c_s^2}\right]
\tag{2}
$$

$$
\begin{aligned}
T_\alpha^\sigma(\boldsymbol{r} + \boldsymbol{e}_\alpha\delta_t, t + \delta_t) - T_\alpha^\sigma(\boldsymbol{r}, t) \\
= -\frac{1}{\tau_T^\sigma}\left[T_\alpha^\sigma(\boldsymbol{r}, t) - T_{\alpha^{\sigma eq}}(\boldsymbol{r}, t)\right]
\end{aligned}
\tag{3}
$$

$$
T_\alpha^{\sigma eq} = w_\alpha T^\sigma \left[1 + 3\frac{\boldsymbol{e}_\alpha \cdot \boldsymbol{u}^\sigma}{c^2} + 4.5\frac{(\boldsymbol{e}_\alpha \cdot \boldsymbol{u}^\sigma)^2}{2c^4} - 1.5\frac{u^{\sigma 2}}{2c^2}\right]
\tag{4}
$$

The interaction forces including gravity and buoyancy force F_H, drag force F_D, interaction potential force F_A, and Brownian force $\boldsymbol{F}_B$ are presented respectively as follows:

Table 2 Grid independence test. Numerical simulation results at different grids ($Ra = 1 \times 10^5$, $\varphi = 0.05$)

Grid number	78 × 39	128 × 64	198 × 99	256 × 128	300 × 150
Nu_{avg}	1.583	1.770	1.789	1.805	1.806

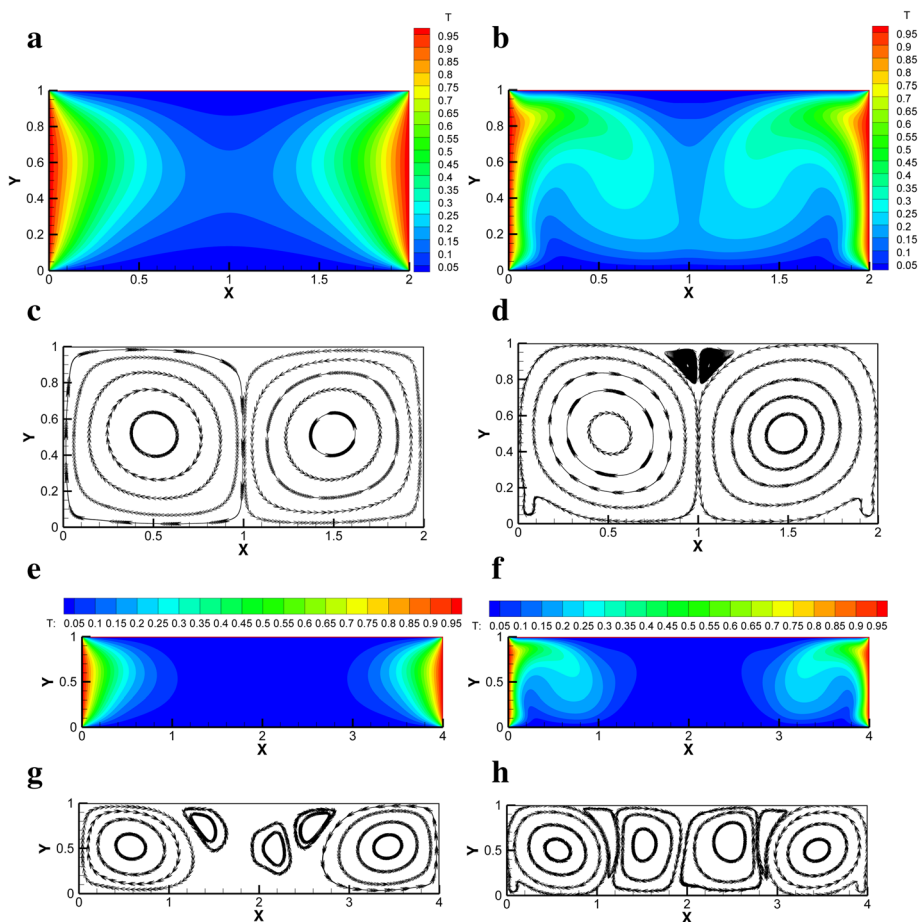Qi *et al. Nanoscale Research Letters* (2017) 12:326

Page 3 of 10

Fig. 2 Temperature nephogram and streamlines of Ag-Ga nanofluid. Temperature nephogram and streamlines of Ag-Ga nanofluid ($r = 20$ nm, $\varphi = 0.01$) in the horizontal rectangular enclosure ($A = 2$:1 and $A = 4$:1). Temperature nephogram: **a** $Ra = 1 \times 10^3$, $A = 2$:1. **b** $Ra = 1 \times 10^5$, $A = 2$:1. **e** $Ra = 1 \times 10^3$, $A = 4$:1. **f** $Ra = 1 \times 10^5$, $A = 4$:1. Streamlines: **c** $Ra = 1 \times 10^3$, $A = 2$:1. **d** $Ra = 1 \times 10^5$, $A = 2$:1. **g** $Ra = 1 \times 10^3$, $A = 4$:1. **h** $Ra = 1 \times 10^5$, $A = 4$:1
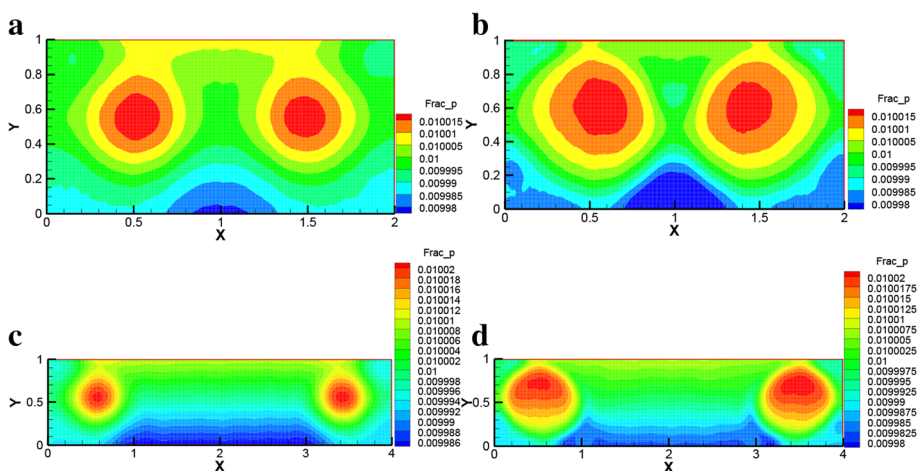

Fig. 3 Nanoparticle volume fraction distributions of Ag-Ga nanofluid. Nanoparticle volume fraction distributions of Ag-Ga nanofluid ($r = 20$ nm, $\varphi = 0.01$) in the horizontal rectangular enclosure ($A = 2$:1 and $A = 4$:1). **a** $Ra = 1 \times 10^3$, $A = 2$:1. **b** $Ra = 1 \times 10^5$, $A = 2$:1. **c** $Ra = 1 \times 10^3$, $A = 4$:1. **d** $Ra = 1 \times 10^5$, $A = 4$:1

Qi *et al. Nanoscale Research Letters* (2017) 12:326

Page 4 of 10

$$F_{\mathrm{H}} = -\frac{4\pi a^3}{3} g \Delta \rho' \tag{5}$$

$$F_{\mathrm{D}} = -6\pi \mu a \Delta u \tag{6}$$

$$F_{\mathrm{A}} = \sum_{i=1}^{8} n_i \frac{\partial V_{\mathrm{A}}}{\partial r_i} \tag{7}$$

$$F_{\mathrm{B}} = G_i \sqrt{\frac{C}{dt}} \tag{8}$$

All units in the simulation adopt the lattice units. The transformation relationships between lattice units and international units are as follows:

$$\begin{cases} t' = \dfrac{t}{T}, \ \ l' = \dfrac{l}{L}, \ \ u' = u\dfrac{T}{L} = u\dfrac{v'}{v}\dfrac{D}{D'}, \ \ a' = a\dfrac{T^2}{L} = a\left(\dfrac{v'}{v}\right)^2 \left(\dfrac{D}{D'}\right)^3 \\ m' = \dfrac{m}{G} = m\dfrac{\rho'}{\rho}\left(\dfrac{D}{D'}\right)^3, \ \ F' = F\dfrac{T^2}{GL} = F\dfrac{\rho'}{\rho}\left(\dfrac{v'}{v}\right)^2 \end{cases} \tag{9}$$

where the physical quantities with the superscript "'" represent the lattice units and the physical quantities without the superscript "'" represent the international units.

The other details of this model can be seen in the previous published paper [31].

Results and Discussion

Figure 1 presents the horizontal rectangular enclosure filled with Ag-Ga nanofluid in the simulation. The aspect ratio between width and height is defined as $A = W/H$. The thermo-physical parameters of liquid metal gallium (Ga) and silver (Ag) nanoparticles are given in Table 1. Because the temperature change has a great effect on the specific heat of Ga while a mall effect on the specific heat of Ag, in order to simplify the calculation, the specific heat of Ga considers the effect of temperature, and the specific heat of Ag keeps a constant. The left and right walls of the horizontal rectangular enclosure are all hot wall T_{H}, and the top and bottom walls are all cold wall T_{C}. The initialization conditions of the four walls are shown as follows:

$$\begin{cases} x = 0 \quad u = 0, \quad T = 1; \quad x = 1 \quad u = 0, \quad T = 1 \\ y = 0 \quad u = 0, \quad T = 0; \quad y = 1 \quad u = 0, \quad T = 0 \end{cases} \tag{10}$$

Before the study in Ag-Ga nanofluid, a grid independence test is analyzed. Five kinds of grids (78×39, 128×64, 198×99, 256×128, and 300×150) are chosen to be tested in this paper. The results under different grids are showed in Table 2. It can be seen from Table 2 that there are noticeable differences in the results from 78×39 to 256×128 but few differences from 256×128 to 300×150. In order to accelerate the numerical simulation velocity, the grid 256×128 is adopted for $A = 2:1$

Table 3 Ranges of driving force and interaction forces, $A = 2:1$. Ranges of driving force and interaction forces between particles in the nanofluid ($A = 2:1$, $Ra = 10^5$, $\varphi = 0.01$)

Forces	$r = 20$ nm	$r = 40$ nm	$r = 80$ nm
F_{S}	−1.2E−5 ~ 1.2E−5	−1.2E−5 ~ 1.2E−5	−1.2E−5 ~ 1.2E−5
F_{A}	−3.2E−19 ~ −2E−20	−8E−19 ~ −5E−20	−2.8E−18 ~ −2E−19
F_{Bx}	−5E−13 ~ 5E−13	−5E−13 ~ 5E−13	−5E−13 ~ 5E−13
F_{By}	2E−14 ~ 2E−13	2E−14 ~ 2E−13	2E−14 ~ 2E−13
F_{H}	−9E−19 ~ −1E−19	−7.5E−18 ~ −5E−19	−6E−17 ~ −5E−18
F_{Dx}	−7E−15 ~ 7E−15	−1.2E−14 ~ 1.2E−14	−2E−14 ~ 2E−14
F_{Dy}	−8E−15 ~ 7E−15	−1.4E−14 ~ 1.2E−14	−2E−14 ~ 2E−14

enclosure in this numerical simulation. Correspondingly, the grid 256×64 is adopted for $A = 4:1$ enclosure.

The reliability and accuracy of the two-phase lattice Boltzmann model have been verified in the previous published paper [31].

Figure 2 shows the temperature nephogram and streamlines of Ag-Ga nanofluid ($r = 20$ nm, $\varphi = 0.01$) in the horizontal rectangular enclosure ($A = 2:1$ and $A = 4:1$) at different Rayleigh numbers ($Ra = 1 \times 10^3$ and $Ra = 1 \times 10^5$) respectively. It can be seen that the isotherm becomes more and more crooked with the Rayleigh number. The number of vortexes in the enclosure increases with the Rayleigh number. The vortexes can disturb the laminar boundary layer and enhance the heat transfer. The main heat transfer form is heat conduction at low Rayleigh number $Ra = 1 \times 10^3$, while the main heat transfer form changes from heat conduction to convection heat transfer at high Rayleigh number $Ra = 1 \times 10^5$. High Rayleigh number causes a big temperature difference driving force which disturbs the laminar boundary layer and improves the heat transfer compared with the low Rayleigh number.

Figure 3 presents the nanoparticle volume fraction distributions of Ag-Ga nanofluid ($r = 20$ nm, $\varphi = 0.01$) in the horizontal rectangular enclosure at different Rayleigh numbers ($Ra = 1 \times 10^3$ and $Ra = 1 \times 10^5$) respectively. It can be seen from Fig. 3 that the high nanoparticle volume fraction mainly distributes in the left and right sides (the center of the vortexes) of the enclosure. The velocity in

Table 4 Ranges of driving force and interaction forces, $A = 4:1$. Ranges of driving force and interaction forces between particles in the nanofluid ($A = 4:1$, $Ra = 10^5$, $\varphi = 0.01$)

Forces	$r = 20$ nm	$r = 40$ nm	$r = 80$ nm
F_{S}	−2.5E−5 ~ 2.5E−5	−2.5E−5 ~ 2.5E−5	−2.5E−5 ~ 2.5E−5
F_{A}	−3.2E−19 ~ −2E−20	−8E−19 ~ −5E−20	−2.8E−18 ~ −2E−19
F_{Bx}	−5E−13 ~ 5E−13	−5E−13 ~ 5E−13	−5E−13 ~ 5E−13
F_{By}	2E−14 ~ 2E−13	2E−14 ~ 2E−13	2E−14 ~ 2E−13
F_{H}	−9.5E−19 ~ −5E−20	−7.5E−18 ~ −5E−19	−6E−17 ~ −5E−18
F_{Dx}	−7E−15 ~ 7E−15	−1.2E−14 ~ 1.6E−14	−2.5E−14 ~ 2.5E−14
F_{Dy}	−8E−15 ~ 7E−15	−1.4E−14 ~ 1.2E−14	−2E−14 ~ 2E−14

Qi *et al. Nanoscale Research Letters* (2017) 12:326
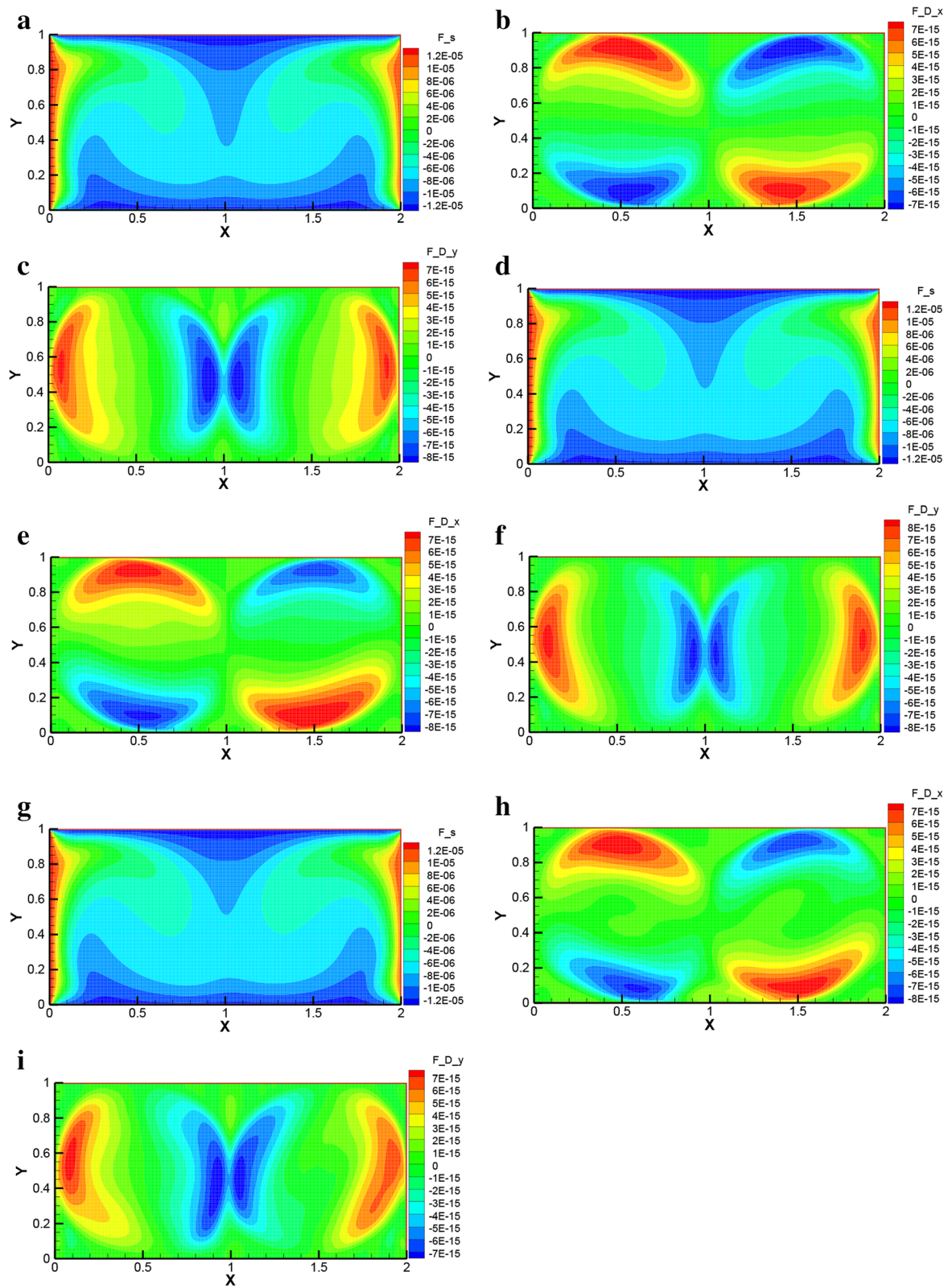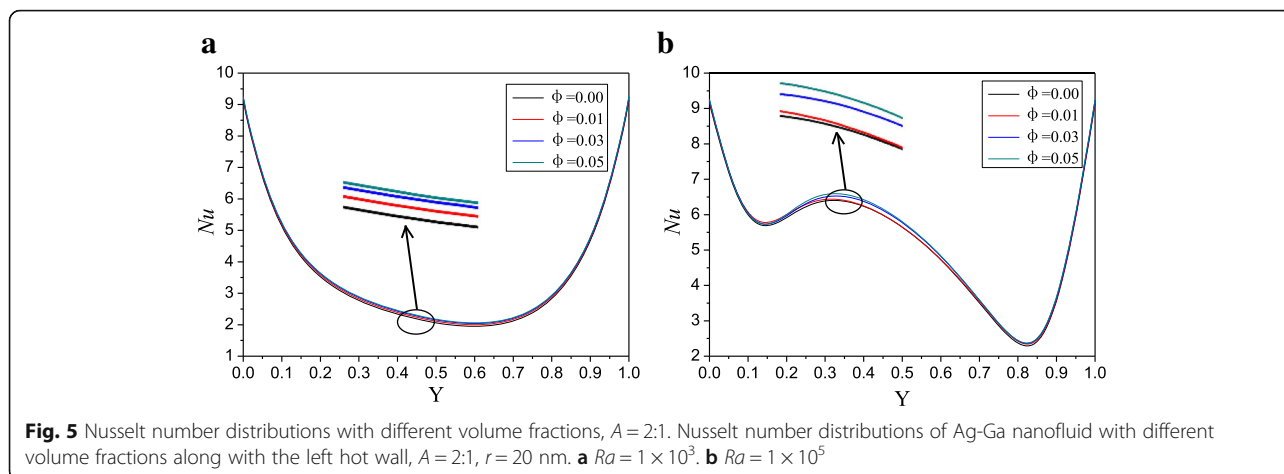
Page 5 of 10

Fig. 4 Temperature difference driving force F_S and drag force F_D. Temperature difference driving force F_S and drag force F_D at $Ra = 1 \times 10^5$ ($A = 2{:}1$, $r = 20$ nm). **a** F_S, $\varphi = 0.01$. **b** F_{Dx}, $\varphi = 0.01$. **c** F_{Dy}, $\varphi = 0.01$. **d** F_S, $\varphi = 0.03$. **e** F_{Dx}, $\varphi = 0.03$. **f** F_{Dy}, $\varphi = 0.03$. **g** F_S, $\varphi = 0.05$. **h** F_{Dx}, $\varphi = 0.05$. **i** F_{Dy}, $\varphi = 0.05$

Fig. 5 Nusselt number distributions with different volume fractions, $A = 2:1$. Nusselt number distributions of Ag-Ga nanofluid with different volume fractions along with the left hot wall, $A = 2:1$, $r = 20$ nm. **a** $Ra = 1 \times 10^3$. **b** $Ra = 1 \times 10^5$
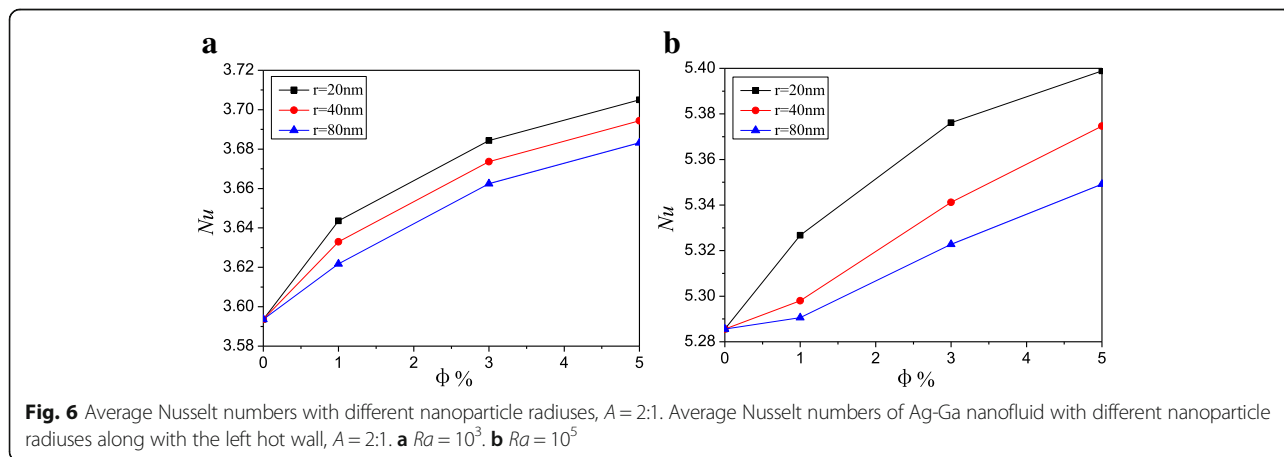
the center of the vortex is smaller than that outside of vortexes. Due to the smaller velocity of nanoparticles compared with water, the nanoparticles mainly fall into the center of the two big vortexes in the left and right sides of the enclosure.
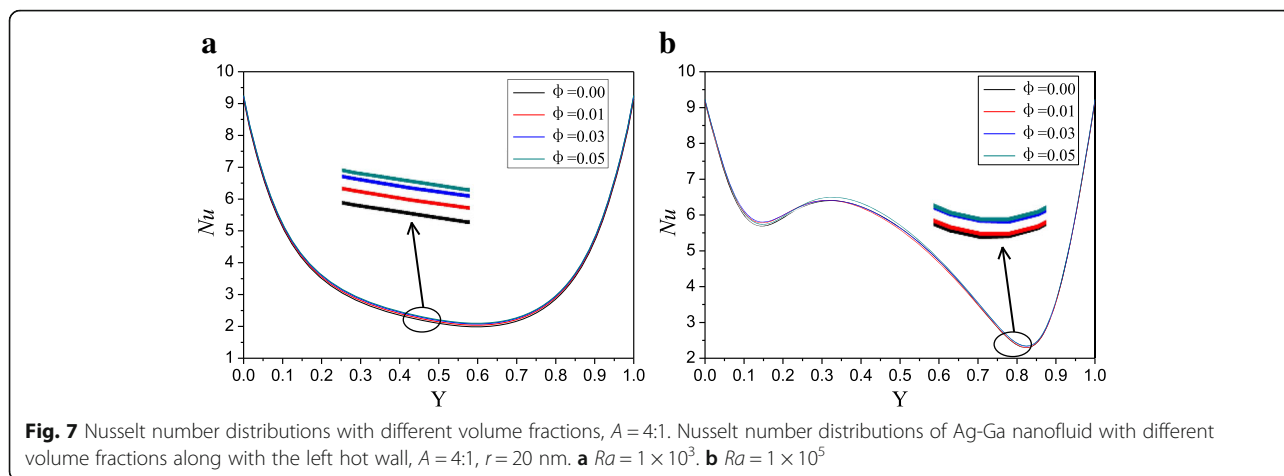
There are driving force F_S and interaction forces between particles including gravity and buoyancy force F_H, drag force (Stokes force) F_D, interaction potential force F_A, and Brownian force F_B for nanofluid. For $Ra = 10^5$ and $\phi = 0.01$, the ranges of interaction forces between particles in enclosure with $A = 2:1$ and $A = 4:1$ are given in Tables 3 and 4 respectively. It can be seen from these two tables that the driving force F_S is the biggest force, and among the interaction forces between particles, Brownian force F_B is the biggest force, followed by the drag force F_D. It can be also seen that Brownian force F_B is about two magnitudes greater than drag force F_D, which is another reason for the enhancement of nanofluid in addition to the high thermal conductivity of nanofluid. In addition, it can be obtained a conclusion that the values of the driving force F_S in enclosure ($A = 4:1$) are about twice the values of F_S in enclosure ($A = 2:1$) while those of the other forces are almost the

same, which causes a higher heat transfer enhancement ratio in enclosure with $A = 4:1$ compared with that in enclosure with $A = 2:1$.

Figure 4 shows the biggest advantageous force F_S and the biggest disadvantageous force F_D distributions at high Rayleigh number $Ra = 1 \times 10^5$ ($A = 2:1$, $r = 20$ nm). It can be seen that the driving force F_S distribution is similar to the temperature distribution. This is because the driving force F_S is the biggest force and plays a main role in the temperature distribution. The drag force F_D mainly surrounds the border of the vortex in the enclosure. This is because the velocity of nanofluid and the corresponding velocity difference between nanoparticle and gallium surrounding the border of the vortex are all bigger than that in other places.

Take the nanoparticle radius $r = 20$ nm and the aspect ratio of enclosure $A = 2:1$, for example, Figs. 5 and 6 give the Nusselt number distributions and average Nusselt numbers of Ag-Ga nanofluid with different nanoparticle volume fractions along with the left hot wall at different Rayleigh numbers respectively. It can be seen from Fig. 5 that Nusselt number increases with the nanoparticle
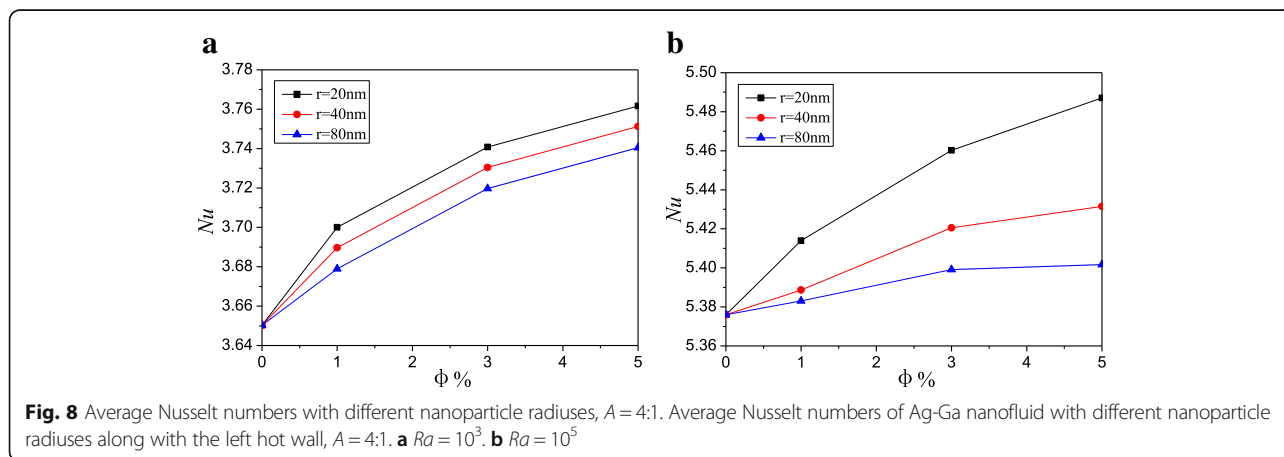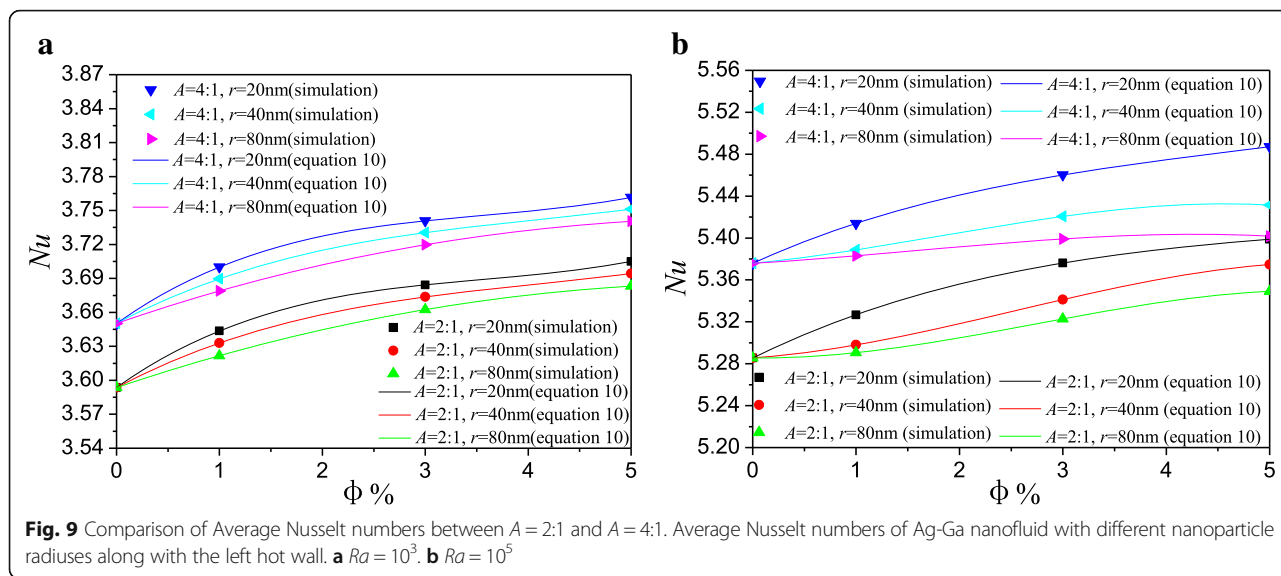

Fig. 6 Average Nusselt numbers with different nanoparticle radiuses, $A = 2:1$. Average Nusselt numbers of Ag-Ga nanofluid with different nanoparticle radiuses along with the left hot wall, $A = 2:1$. **a** $Ra = 10^3$. **b** $Ra = 10^5$

Qi *et al. Nanoscale Research Letters* (2017) 12:326

Page 7 of 10

Fig. 7 Nusselt number distributions with different volume fractions, $A = 4:1$. Nusselt number distributions of Ag-Ga nanofluid with different volume fractions along with the left hot wall, $A = 4:1$, $r = 20$ nm. **a** $Ra = 1 \times 10^3$. **b** $Ra = 1 \times 10^5$

volume fraction. High nanoparticle volume fraction can enhance the whole thermal conductivity of nanofluid and improve the natural convection heat transfer. It can be also seen from Fig. 5 that the Nusselt number firstly decreases with Y and then increases with Y, and there is only one Nusselt number valley at low Rayleigh number. However, there are two Nusselt number valleys at high Rayleigh number. At low Rayleigh number, there are no obvious vortexes between the two big vortexes (Fig. 2c), and the velocity in the place between the two big vortexes is small, which causes small Nusselt numbers. At high Rayleigh number, there are two small vortexes between the two big vortexes (Fig. 2d), which disturb the laminar boundary layer and enhance the Nusselt number. Hence, there are two Nusselt number valleys at high Rayleigh number, while there is only one Nusselt number valley at low Rayleigh number, and it shows a more fluctuation in the Nusselt number distributions along with the left hot wall in Fig. 5b compared with that in Fig. 5a. It can be seen from Fig. 6 that Nusselt number increases with the decrease of the nanoparticle radius. For $A = 2:1$, Ag-Ga nanofluid with the smallest

nanoparticle radius ($r = 20$ nm) can enhance the heat transfer by 3.1 and 2.1% compared with water at $Ra = 10^3$ and $Ra = 10^5$ respectively.

The similar conclusions can be obtained from Figs. 7 and 8 compared with Figs. 5 and 6. For $A = 4:1$, Ag-Ga nanofluid with the smallest nanoparticle radius ($r = 20$ nm) can enhance the heat transfer by 3.1 and 2.1% compared with water at $Ra = 10^3$ and $Ra = 10^5$ respectively. The enhancement ratios of the two enclosures ($A = 4:1$ and $A = 2:1$) filled with Ag-Ga nanofluid ($r = 20$ nm) are the same.

Figure 9 shows the average Nusselt numbers of Ag-Ga nanofluid with different nanoparticle radiuses along with the left hot wall. Based on these data in Fig. 9, a mathematic correlation between average Nusselt number and nanoparticle volume fraction is given in Eq. (11). The simulation results and the results in Eq. (11) are all shown in Fig. 9. They have a good agreement with each other. It is found that the more flat horizontal rectangular enclosure (aspect ratio $A = 4:1$) has the higher Nusselt number than the less flat horizontal rectangular enclosure (aspect ratio $A = 2:1$). For every nanoparticle

Fig. 8 Average Nusselt numbers with different nanoparticle radiuses, $A = 4:1$. Average Nusselt numbers of Ag-Ga nanofluid with different nanoparticle radiuses along with the left hot wall, $A = 4:1$. **a** $Ra = 10^3$. **b** $Ra = 10^5$

Qi *et al. Nanoscale Research Letters* (2017) 12:326

Page 8 of 10

Fig. 9 Comparison of Average Nusselt numbers between A = 2:1 and A = 4:1. Average Nusselt numbers of Ag-Ga nanofluid with different nanoparticle radiuses along with the left hot wall. **a** $Ra = 10^3$. **b** $Ra = 10^5$

volume fraction, Nusselt numbers of Ag-Ga nanofluid with the smallest nanoparticle radius (r = 20 nm) in enclosure (A = 4:1) are all 1.5% higher than that in enclosure (A = 2:1) at low Rayleigh number $Ra = 10^3$. Nusselt numbers of nanofluid (r = 20 nm) in enclosure (A = 4:1) are 1.6, 1.1, and 1.0% higher than that in enclosure (A = 2:1) for ϕ = 5%, ϕ = 3%, and ϕ = 1% at high Rayleigh number $Ra = 10^5$ respectively. Big aspect ratio of the horizontal rectangular enclosure in this paper is advantageous to the heat transfer enhancement.

$$Nu_{avg} = a + b\phi + c\phi^2 + d\phi^3 \qquad (11)$$

where $0 \le \phi \le 0.05$ and the constants a, b, c, and d are all shown in the Table 5.

Table 6 shows the Nusselt number enhancement ratios for every nanoparticle radius reducing by half. It can be seen that Nusselt number enhancement ratios for every nanoparticle radius reducing by half are all about 0.3% for two enclosures (A = 2:1 and A = 4:1) at $Ra = 10^3$. This is because the heat conduction plays a major role in the heat transfer, and the Nusselt number enhancement ratios mainly depend on the heat transfer area increment at the same nanoparticle volume fraction. The heat transfer area increment for every nanoparticle radius reducing by half are almost the same, which causes the same Nusselt number enhancement ratios at $Ra = 10^3$. For $Ra = 10^5$, Nusselt number enhancement ratios from the nanoparticle radius r = 80 nm to r = 40 nm for nanofluid (ϕ = 0.1%) in enclosure (A = 2:1 and A = 4:1) are smaller than those in other conditions. At high Rayleigh number $Ra = 10^5$, the convection heat transfer plays a major role in the heat transfer, due to the low nanoparticle volume fraction (ϕ = 1%) and the small heat transfer

Table 5 The constant parameters in Eq. (11). The constant parameters in Eq. (11) at different Rayleigh numbers, aspect ratios, and radiuses

Rayleigh number	Aspect ratio	Radius	a	b	c	d
$Ra = 10^3$	A = 2:1	r = 20 nm	3.59358	0.06429	−0.01577	0.00147
		r = 40 nm	3.59358	0.04796	−0.00939	7.64995E−5
		r = 80 nm	3.59358	0.03084	−0.00269	−2.08674E−5
	A = 4:1	r = 20 nm	3.65026	0.06397	−0.01564	0.00146
		r = 40 nm	3.65026	0.04806	−0.00941	7.68036E−4
		r = 80 nm	3.65026	0.03163	−0.00299	5.39622E−5
$Ra = 10^5$	A = 2:1	r = 20 nm	5.28555	0.04797	−0.00721	4.30087E−4
		r = 40 nm	5.28555	0.00677	0.00651	−8.59108E−4
		r = 80 nm	5.28555	−0.00136	0.00725	−8.87629E−4
	A = 4:1	r = 20 nm	5.37596	0.04436	−0.00691	4.97021E−4
		r = 40 nm	5.37596	0.00938	0.00406	−7.42333E−4
		r = 80 nm	5.37596	0.00554	0.00195	−4.0572E−4

Qi *et al. Nanoscale Research Letters* (2017) 12:326

Page 9 of 10

Table 6 Nusselt number enhancement ratios. Nusselt number enhancement ratios for every nanoparticle radius reducing by half

A	φ	$Ra = 10^3$ $\frac{Nu_{r=20} - Nu_{r=40}}{Nu_{r=40}}$	$Ra = 10^3$ $\frac{Nu_{r=40} - Nu_{r=80}}{Nu_{r=80}}$	$Ra = 10^5$ $\frac{Nu_{r=20} - Nu_{r=40}}{Nu_{r=40}}$	$Ra = 10^5$ $\frac{Nu_{r=40} - Nu_{r=80}}{Nu_{r=80}}$
2:1	1%	0.3%	0.3%	0.54%	0.14%
	3%	0.28%	0.3%	0.65%	0.35%
	5%	0.29%	0.3%	0.45%	0.48%
4:1	1%	0.29%	0.29%	0.47%	0.10%
	3%	0.28%	0.29%	0.73%	0.40%
	5%	0.28%	0.29%	1.0%	0.56%

area for $r = 80$ nm and $r = 40$ nm; the Nusselt number enhancement ratios are smaller compared with those of the others. Except above two conditions, the Nusselt number enhancement ratios at $Ra = 10^5$ are all higher than those at $Ra = 10^3$. High Rayleigh number can enhance the disturbance and improve the heat transfer.

Conclusions

The natural convection heat transfer of Ag-Ga nanofluid with different nanoparticle radiuses in horizontal rectangle enclosures with different aspect ratios is simulated based on a two-phase lattice Boltzmann model. Some conclusions are obtained as follows:

1. Nusselt number increases with the decrease of the nanoparticle radius. The Nusselt number enhancement ratios of two enclosures ($A = 4:1$ and $A = 2:1$) filled with Ag-Ga nanofluid ($r = 20$ nm) are the same compared with those of the water at the corresponding enclosure. For both $A = 4:1$ and $A = 2:1$, Ag-Ga nanofluid with the smallest nanoparticle radius ($r = 20$ nm) can enhance the heat transfer by 3.1 and 2.1% at best compared with water at $Ra = 10^3$ and $Ra = 10^5$ respectively.
2. The more flat horizontal rectangular enclosure ($A = 4:1$) has the higher Nusselt number than the less flat horizontal rectangular enclosure ($A = 2:1$). Nusselt numbers of Ag-Ga nanofluid ($r = 20$ nm) in the enclosure ($A = 4:1$) are all 1.5% higher than those in enclosure ($A = 2:1$) for every nanoparticle volume fraction at $Ra = 10^3$. For $Ra = 10^5$, Nusselt numbers of the enclosure ($A = 4:1$) are 1.0, 1.1, and 1.6% higher than those in enclosure ($A = 2:1$) for $\phi = 1\%$, $\phi = 3\%$, and $\phi = 5\%$ respectively.
3. Nusselt number enhancement ratios for every nanoparticle radius reducing by half at high Rayleigh number are higher than those at low Rayleigh number in most cases. For the two enclosures ($A = 2:1$ and $A = 4:1$), Nusselt number enhancement ratios for every nanoparticle radius reducing by half are all about 0.3% at $Ra = 10^3$, and most of them are 0.35 to 1.0% at $Ra = 10^5$.

4. The Brownian force F_B is about two magnitudes greater than the drag force F_D. The value of driving force F_S in $A = 4:1$ enclosure is about twice the value of driving force F_S in $A = 2:1$ enclosure while other forces are almost the same.

Authors' Contributions
CQ participated in the design of the program, carried out the numerical simulation of the nanofluid, and drafted the manuscript. LYY and GQW participated in the design of the program. All authors read and approved the final manuscript.

References
1. Li H, Wang L, He Y, Hu Y, Zhu J, Jiang B (2015) Experimental investigation of thermal conductivity and viscosity of ethylene glycol based ZnO nanofluids. Appl Therm Eng 88:363–368
2. Chen M, He Y, Zhu J, Shuai Y, Jiang B, Huang Y (2015) An experimental investigation on sunlight absorption characteristics of silver nanofluids. Sol Energy 115:85–94
3. Yang JC, Li FC, Zhou WW, He Y, Jiang B (2012) Experimental investigation on the thermal conductivity and shear viscosity of viscoelastic-fluid-based nanofluids. Int J Heat Mass Transfer 55(11):3160–3166
4. Yang JC, Li FC, He YR, Huang YM, Jiang BC (2013) Experimental study on the characteristics of heat transfer and flow resistance in turbulent pipe flows of viscoelastic-fluid-based Cu nanofluid. Int J Heat Mass Transfer 62: 303–313
5. Yang JC, Li FC, Cai WH, Zhang HN, Yu B (2014) On the mechanism of convective heat transfer enhancement in a turbulent flow of nanofluid investigated by DNS and analyses of POD and FSP. Int J Heat Mass Transfer 78:277–288
6. Li H, He Y, Hu Y, Jiang B, Huang Y (2015) Thermophysical and natural convection characteristics of ethylene glycol and water mixture based ZnO nanofluids. Int J Heat Mass Transfer 91:385–389
7. He Y, Li H, Hu Y, Hu Y, Wang X, Zhu J (2016) Boiling heat transfer characteristics of ethylene glycol and water mixture based ZnO nanofluids in a cylindrical vessel. Int J Heat Mass Transfer 98:611–615
8. Ho CJ, Chang CY, Cheng CY, Cheng SJ, Guo YW, Hsu ST, Yan WM (2016) Laminar forced convection effectiveness of Al₂O₃–water nanofluid flow in a circular tube at various operation temperatures: effects of temperature-dependent properties. Int J Heat Mass Transfer 100:464–481
9. He Y, Qi C, Hu Y, Qin B, Ding Y (2011) Lattice Boltzmann simulation of alumina-water nanofluid in a square cavity. Nanoscale Res Lett 6(1):184–191
10. Ho CJ, Liu WK, Chang YS, Lin CC (2010) Natural convection heat transfer of alumina-water nanofluid in vertical square enclosures: an experimental study. Int J Therm Sci 49(8):1345–1353
11. Heris SZ, Etemad SG, Esfahany MN (2006) Experimental investigation of oxide nanofluids laminar flow convective heat transfer. Int Commun Heat Mass Transfer 33(4):529–535
12. Heris SZ, Esfahany MN, Etemad SG (2007) Experimental investigation of convective heat transfer of Al₂O₃/water nanofluid in circular tube. Int J Heat Fluid Flow 28(2):203–210
13. Heris SZ, Etemad SG, Esfahany MN (2009) Convective heat transfer of a Cu/water nanofluid flowing through a circular tube. Exp heat transfer 22(4): 217–227

Qi *et al. Nanoscale Research Letters* (2017) 12:326

Page 10 of 10

14. Hu Y, He Y, Wang S, Wang Q, Schlaberg HI (2014) Experimental and numerical investigation on natural convection heat transfer of TiO_2–water nanofluids in a square enclosure. J Heat Transfer 136(2):022502

15. Sommers AD, Yerkes KL (2010) Experimental investigation into the convective heat transfer and system-level effects of Al_2O_3-propanol nanofluid. J Nanopart Res 12(3):1003–1014

16. He Y, Men Y, Zhao Y, Lu H, Ding Y (2009) Numerical investigation into the convective heat transfer of TiO_2 nanofluids flowing through a straight tube under the laminar flow conditions. Appl Therm Eng 29(10):1965–1972

17. Bianco V, Chiacchio F, Manca O, Nardini S (2009) Numerical investigation of nanofluids forced convection in circular tubes. Appl Therm Eng 29(17): 3632–3642

18. Bianco V, Manca O, Nardini S (2011) Numerical investigation on nanofluids turbulent convection heat transfer inside a circular tube. Int J Therm Sci 50(3):341–349

19. Bianco V, Manca O, Nardini S (2014) Performance analysis of turbulent convection heat transfer of Al_2O_3 water-nanofluid in circular tubes at constant wall temperature. Energy 77:403–413

20. Akbarinia A, Behzadmehr A (2007) Numerical study of laminar mixed convection of a nanofluid in horizontal curved tubes. Appl Therm Eng 27(8): 1327–1337

21. Moghari RM, Akbarinia A, Shariat M, Talebi F, Laur R (2011) Two phase mixed convection Al_2O_3–water nanofluid flow in an annulus. Int J Multiphase Flow 37(6):585–595

22. Shariat M, Akbarinia A, Nezhad AH, Behzadmehr A, Laur R (2011) Numerical study of two phase laminar mixed convection nanofluid in elliptic ducts. Appl Therm Eng 31(14):2348–2359

23. Sheikholeslami M, Gorji-Bandpy M, Vajravelu K (2015) Lattice Boltzmann simulation of magnetohydrodynamic natural convection heat transfer of Al_2O_3–water nanofluid in a horizontal cylindrical enclosure with an inner triangular cylinder. Int J Heat Mass Transfer 80:16–25

24. Sheikholeslami M, Ellahi R (2015) Three dimensional mesoscopic simulation of magnetic field effect on natural convection of nanofluid. Int J Heat Mass Transfer 89:799–808

25. Sheikholeslami M, Vajravelu K, Rashidi MM (2016) Forced convection heat transfer in a semi annulus under the influence of a variable magnetic field. Int J Heat Mass Transfer 92:339–348

26. Sheikholeslami M, Chamkha AJ (2016) Flow and convective heat transfer of a ferro-nanofluid in a double-sided lid-driven cavity with a wavy wall in the presence of a variable magnetic field. Numer Heat Transfer, Part A: Appl 69(10):1186–1200

27. Sheikholeslami M, Rashidi MM (2015) Ferrofluid heat transfer treatment in the presence of variable magnetic field. Eur Phys J Plus 130(6):1–12

28. Qi C, He G, Li Y, He Y (2015) Numerical simulation of natural convection of square enclosure filled with Cu/Al_2O_3–water mixed nanofluid based on lattice Boltzmann method. Acta Phys Sin 64(2):024703 (in Chinease)

29. Qi C, He Y, Yan S, Tian F, Hu Y (2013) Numerical simulation of natural convection in a square enclosure filled with nanofluid using the two-phase lattice Boltzmann method. Nanoscale Res Lett 8(1):1–16

30. Qi C, He Y, Hu Y, Yang J, Li F, Ding Y (2011) Natural convection of Cu-gallium nanofluid in enclosures. J Heat Transfer 133(12):122504

31. Qi C, Liang L, Rao Z (2016) Study on the flow and heat transfer of liquid metal based nanofluid with different nanoparticle radiuses using two-phase lattice Boltzmann method. Int J Heat Mass Transfer 94:316–326

32. Vajravelu K, Prasad KV, Lee J, Lee C, Pop I, Gorder RAV (2011) Convective heat transfer in the flow of viscous Ag–water and Cu–water nanofluids over a stretching surface. Int J Therm Sci 50(5):843–851